LLNL-JRNL-2007049

Lawrence Livermore National Laboratory

Delving into the depths of NGC 3783 with XRISM I. Kinematic and ionization structure of the highly ionized outflows

M Mehdipour, K Hagino, T Kallman, E Kara, C Li, J Miller, M Mizumoto, H Noda, S Ogawa, C Panagiotou, A Tanimoto, J Kaastra, K Zhao, M Eckart, L Gu, R Ballhausen, E Behar, C Diez, K Fukumura, M Guainazzi

September 2025

Astronomy and Astrophysics

Disclaimer

This work performed under the auspices of the U.S. Department of Energy by Lawrence Livermore National Laboratory under Contract DE-AC52-07NA27344.

Astronomy & Astrophysics manuscript no. Paper_I
June 11, 2025

Delving into the depths of NGC 3783 with XRISM

I. Kinematic and ionization structure of the highly ionized outflows

Missagh Mehdipour[1], Jelle S. Kaastra[2,3], Megan E. Eckart[4], Liyi Gu[2,3], Ralf Ballhausen[5,6,7], Ehud Behar[8,9], Camille M. Diez[10], Keigo Fukumura[11], Matteo Guainazzi[12], Kouichi Hagino[13], Timothy R. Kallman[6], Erin Kara[9], Chen Li[3,2], Jon M. Miller[14], Misaki Mizumoto[15], Hirofumi Noda[16], Shoji Ogawa[17], Christos Panagiotou[9], Atsushi Tanimoto[18], and Keqin Zhao[3,2]

[1] Space Telescope Science Institute, 3700 San Martin Drive, Baltimore, MD 21218, USA
e-mail: missagh.mehdipour@gmail.com
[2] SRON Netherlands Institute for Space Research, Niels Bohrweg 4, 2333 CA Leiden, the Netherlands
[3] Leiden Observatory, Leiden University, PO Box 9513, 2300 RA Leiden, the Netherlands
[4] Lawrence Livermore National Laboratory, Livermore, CA 94550, USA
[5] University of Maryland College Park, Department of Astronomy, College Park, MD 20742, USA
[6] NASA Goddard Space Flight Center (GSFC), Greenbelt, MD 20771, USA
[7] Center for Research and Exploration in Space Science and Technology, NASA GSFC (CRESST II), Greenbelt, MD 20771, USA
[8] Department of Physics, Technion, Haifa 32000, Israel
[9] MIT Kavli Institute for Astrophysics and Space Research, Massachusetts Institute of Technology, Cambridge, MA 02139, USA
[10] ESA European Space Astronomy Centre (ESAC), Camino Bajo del Castillo s/n, 28692 Villanueva de la Cañada, Madrid, Spain
[11] Department of Physics and Astronomy, James Madison University, Harrisonburg, VA 22807, USA
[12] ESA European Space Research and Technology Centre (ESTEC), Keplerlaan 1, 2201 AZ, Noordwijk, the Netherlands
[13] Department of Physics, University of Tokyo, 7-3-1 Hongo, Bunkyo-ku, Tokyo 113-0033, Japan
[14] Department of Astronomy, University of Michigan, 1085 South University Avenue, Ann Arbor, MI, 48109, USA
[15] Science Research Education Unit, University of Teacher Education Fukuoka, Munakata, Fukuoka 811-4192, Japan
[16] Astronomical Institute, Tohoku University, 6-3 Aramakiazaaoba, Aoba-ku, Sendai, Miyagi 980-8578, Japan
[17] Institute of Space and Astronautical Science (ISAS), Japan Aerospace Exploration Agency (JAXA), Kanagawa 252-5210, Japan
[18] Graduate School of Science and Engineering, Kagoshima University, Kagoshima, 890-8580, Japan

Received 21 May 2025 / Accepted 11 June 2025

ABSTRACT

We present our study of the X-Ray Imaging and Spectroscopy Mission (XRISM) observation of the Seyfert-1 galaxy NGC 3783. For the first time, XRISM's Resolve microcalorimeter enables a detailed characterization of the highly ionized outflows in this active galactic nucleus. Our analysis constrains their outflow and turbulent velocities, along with their ionization parameter ξ and column density $N_{\rm H}$. The high-resolution Resolve spectrum reveals a distinct series of Fe absorption lines between 6.4 and 7.8 keV, ranging from Fe XVIII to Fe XXVI. At lower energies (1.8–3.3 keV), absorption features from Si, S, and Ar are also detected. Our spectroscopy and photoionization modeling of the time-averaged Resolve spectrum uncover six outflow components, five of which exhibit relatively narrow absorption lines, with outflow velocities ranging from 560 to 1170 km s^{-1}. In addition, a broad absorption feature is detected, which is consistent with Fe XXVI outflowing at 14,300 km s^{-1} (0.05 c). This component carries a kinetic luminosity of 0.8–3% of the bolometric luminosity. Our analysis of the Resolve spectrum shows that more highly ionized absorption lines are intrinsically broader than those of lower ionization species, indicating that the turbulent velocity of the six outflow components (ranging from 0 to 3500 km s^{-1}) increases with ξ. Furthermore, we find that the column density $N_{\rm H}$ of the outflows generally declines with the ionization parameter up to $\log\xi = 3.2$, but rises beyond this point, suggesting a complex ionization structure. Examination of the absorption profile of the Fe XXV resonance line reveals intriguing similarities to UV absorption lines (Lyα and C IV) observed by the Hubble Space Telescope, from which we infer that the outflows are clumpy in nature. Our XRISM/Resolve results from lower and higher ionization regimes support a 'hybrid wind' scenario, in which the observed outflows have multiple origins and driving mechanisms. We explore various interpretations of our findings within AGN wind models.

Key words. X-rays: galaxies – galaxies: active – galaxies: Seyfert – galaxies: individual: NGC 3783 – techniques: spectroscopic

1. Introduction

Outflows and winds in active galactic nuclei (AGN) serve as crucial links between supermassive black holes (SMBHs) and their surrounding environments. These outflows carry matter away from the central black hole, dispersing it throughout the host galaxy. This transfer of mass and energy plays a key role in the co-evolution of SMBHs and their galaxies, influencing feedback mechanisms that affect AGN activity and star formation (King & Pounds 2015; Gaspari & Sądowski 2017). Therefore, understanding the physical properties, energetics, and driving mechanisms of AGN winds is essential for determining their role in AGN feedback and evaluating their impact on the interstellar medium (ISM).

The dynamics, kinematics, and ionization structure of ionized outflows, ranging from the vicinity of the accretion disk to the outer regions of the host galaxy, remain poorly understood. This uncertainty makes it difficult to determine how these outflows transfer momentum and energy into the galaxy and influence their surroundings. Ionized outflows (e.g. Laha et al. 2014) have been observed at different scales, each exhibiting distinct characteristics: the micro (sub-pc) scale, associated with the accretion disk and broad-line region (BLR); the meso (pc) scale, linked to the torus and narrow-line region (NLR); and the macro (kpc) scale, extending into the host galaxy (Laha et al. 2021; Gallo et al. 2023). However, the formation mechanisms of these various outflows and their interconnections remain uncertain. Additionally, their connection to galactic molecular outflows is not well understood. Key questions persist regarding the origin of ionized outflows (whether from the disk or torus) and the mechanisms driving them (thermal, radiative, or magnetic). The physical factors that govern the launching and duty cycles of these winds, as well as how wind parameters scale with redshift and AGN properties (e.g. luminosity), remain open questions.

The Resolve microcalorimeter onboard the X-ray Imaging and Spectroscopy Mission (XRISM, Tashiro et al. 2020, 2025) offers an exceptional combination of energy resolution (~ 4.5 eV FWHM) and sensitivity at hard X-ray energies (1.8–12 keV), making it invaluable for studying highly ionized outflows that exhibit X-ray absorption features in the Fe K band (6–8 keV). These outflows can have velocities ranging from moderate (a few hundred km/s) to relativistic speeds (i.e. the ultra-fast outflows; UFOs Tombesi et al. 2010). Studying highly ionized outflows with previous X-ray missions has been challenging due to limitations in both spectral resolution and sensitivity, leading to considerable uncertainties in their kinematics and ionization structure. Consequently, key aspects of the origin, launch mechanisms, and kinetic power of these outflows remain poorly understood. XRISM/Resolve's high resolving power enables detailed probing of these highly ionized outflows, allowing for precise determination of their parameters, as first demonstrated for NGC 4151 by XRISM Collaboration et al. (2024).

The bright Seyfert-1 galaxy NGC 3783, rich in spectral lines, serves as an excellent laboratory for studying ionized outflows in AGN. It is an ideal target for XRISM because it is exceptionally bright in the Fe K band and has previously exhibited evidence of highly ionized outflows, seen as both narrow (Kaspi et al. 2002) and broad (Mehdipour et al. 2017) X-ray absorption features. Additionally, it exhibits a clear and well-defined spectrum of ionized outflows in the soft X-rays (Behar et al. 2003; Mao et al. 2019; Gu et al. 2023; Li et al. 2025) and UV (Gabel et al. 2005; Scott et al. 2014; Kriss et al. 2019). A 900 ks *Chandra*/HETG spectrum revealed a 3σ detection of a narrow Fe xxv resonance line, as well as marginal detections of other transitions (Kaspi et al. 2002; Yaqoob et al. 2005). Evidence for Fe xxv absorption has also been detected in *XMM-Newton*/EPIC spectra (Reeves et al. 2004; Costanzo et al. 2022), suggesting that the highly ionized absorption is variable over time. Remarkably, NGC 3783 also undergoes periods of transient obscuration events caused by disk winds, during which new blueshifted and broad absorption features appear in the Fe K band and the UV HST spectra (Mehdipour et al. 2017).

The XRISM Performance Verification (PV) observation of NGC 3783 started on 2024-07-18 (04:58 UTC) and ended on 2024-07-27 (16:16 UTC). The total exposure of the Resolve spectrum is 439 ks. Fortunately, at the time of our observation, NGC 3783 was particularly bright in X-rays ($F_{2-10\,\mathrm{keV}} = 6.0 \times 10^{-11}$ erg cm^{-2} s^{-1}). Joint simultaneous observations with *XMM-Newton*, *NuSTAR*, *Chandra*, *NICER*, *Swift*, and HST/COS were also performed. In this first paper, we focus exclusively on modeling the XRISM/Resolve spectrum, without incorporating X-ray data from other telescopes. This approach allows us to fully utilize Resolve's unique capability to measure the properties of highly ionized outflows. Further studies of the outflows, incorporating multi-mission spectral modeling, will be presented in future work. Additionally, studies of emission (reflection) and spectral variability are planned for upcoming papers of our campaign.

2. Data reduction and preparation

2.1. XRISM data

Our XRISM observation of NGC 3783 (Obs ID: 300050010) was conducted with the gate valve closed and the open filter wheel configuration of Resolve. A brief summary of the data reduction process and systematic errors is provided below, with more detailed descriptions available in our upcoming cross-calibration paper for NGC 3783 (XRISM Collaboration 2025c, Paper II) as well as in XRISM Collaboration et al. (2025) for PDS 456, which is similar to that of our NGC 3783 observation. We utilized JAXA's pre-pipeline version `004_007.20Jun2024_Build8.012` and pipeline version `03.00.012.008`. Data analysis was performed using the public XRISM `CALDB version 9` (20240815 release) and the `ftools` package, with additional screening and energy-dependent rise time cuts applied according to Mochizuki et al. (2025) and following the XRISM Quick Start Guide Version 2.1. This CALDB includes the initial updates to the Resolve energy scale and line-spread function files based on in-orbit calibration data. After applying good time interval (GTI) filtering, the total effective exposure time was 439 ks.

We selected only the high-resolution primary (Hp) events for our analysis (see Ishisaki et al. 2018 for definition of event grading). The count rate was approximately 0.1 s^{-1} pix^{-1} in the central four pixels and ranged from 0.001 to 0.1 s^{-1} pix^{-1} in the outer pixels, where nearly all astrophysical events are expected to be Hp. To mitigate contamination from "pseudo" low-resolution secondary (Ls) events and corresponding errors in the normalization of the response matrix file (RMF), all Ls events were excluded before generating the RMF (XRISM TTWOF 2025). The RMF was created using the extra-large ("X") option, which includes all known instrumental effects. Gain tracking was performed using 24 fiducial measurements of the Mn Kα line from the ^{55}Fe filter in the filter wheel. Of the 36 pixels, pixel 12 (calibration pixel) and pixel 27 (which exhibits unpredictable gain jumps) were excluded from the analysis.

The instrumental spectroscopic uncertainties that could impact observational results are uncertainties in the broad-band energy scale and the time-dependent gain reconstruction (Eckart et al. 2024; Porter et al. 2024), as well as in the energy resolution. These values have been assessed extensively on the ground and in-orbit. The energy scale uncertainty after gain reconstruction is estimated to be 0.34 eV in the 5.4–8.0 keV band for our observation. This value is based on the ~ 0.16 eV gain reconstruction error at 5.9 keV and the systematic energy scale uncertainty of $\lesssim 0.3$ eV in this band, which are uncorrelated and can be root-sum-squared. The total uncertainty corresponds to 15 km s^{-1} at 7 keV. At energies below 5.4 keV, the total energy scale uncertainty is consistent with $\lesssim 1$ eV, which corresponds to 150 km s^{-1} at 2 keV. The uncertainty on the per-pixel Hp energy resolution values provided in the CALDB is energy-dependent

and estimated to be $\lesssim 0.3$ eV FWHM from 2–10 keV. Its contribution to the systematic uncertainty is smaller than the statistical error on our best-fit model parameters that we present later in Sect. 3 (Table 1).

The preparation of the background-subtracted Resolve spectrum of NGC 3783, including the modeling of the Non-X-ray Background (NXB), as well as the data reduction of Xtend (Noda et al. 2025), is further discussed in a forthcoming paper from our campaign (XRISM Collaboration 2025c, Paper II), which focuses on the cross-calibration of different instruments. For illustration, Fig. A.1 in Appendix A compares the NXB and source spectra, showing that the NXB contribution is minimal in the Resolve spectrum of NGC 3783.

2.2. HST data

Our new HST/COS observations of NGC 3783 (Program ID: 17273) were conducted on 2024-07-21 over two orbits. The COS data were obtained using the G130M and G160M gratings to capture the Lyα and C IV lines. The data were processed with the latest calibration pipeline, `CalCOS v3.6.0`, and the wavelength calibration was verified by checking the observed positions of known Galactic ISM lines. All COS exposures were combined into a single calibrated spectrum, which was then binned by four pixels to improve the signal-to-noise ratio (S/N) while still oversampling the 10-pixel resolution element of the far-UV detector (Fox et al. 2018). For further details on COS data preparation, we refer to the previous HST/COS observation of NGC 3783 in Kriss et al. (2019).

3. Spectral modeling and results

We modeled the time-averaged XRISM/Resolve spectrum (Fig. 1) using `SPEX v3.08.01` (Kaastra et al. 1996; Kaastra et al. 2024) and its latest atomic database. The `rbin` command of `SPEX` was used to optimally bin both the spectrum and the response file, thereby preventing oversampling of the data. The underlying theory and algorithms for `rbin`, which account for both the source statistics and the instrumental resolution, are described in the `SPEX` manual (see also Kaastra & Bleeker 2016). The Resolve spectrum was fitted over the 1.8–12 keV band with C-statistics. The cosmological redshift (`reds`) was fixed at 0.009730 (Theureau et al. 1998), corresponding to a luminosity distance of 41.98 Mpc in `SPEX` based on the cosmological parameters $H_0 = 70$ km s^{-1} Mpc^{-1}, $\Omega_\Lambda = 0.70$, and $\Omega_m = 0.30$. Galactic X-ray absorption was accounted for using the `hot` model (de Plaa et al. 2004; Steenbrugge et al. 2005) in `SPEX`, with the temperature fixed at its minimum value of 0.001 eV, and a column density of $N_\mathrm{H} = 9.59 \times 10^{20}$ cm^{-2} (Murphy et al. 1996). The abundances of all components were set to the protosolar values of Lodders et al. (2009).

3.1. Modeling of the continuum and emission lines

The observed continuum was fitted with a simple power-law model (`pow` in `SPEX`). The intrinsic photon index Γ of the underlying X-ray power-law continuum is found to be $\Gamma = 1.79 \pm 0.01$ from fitting the full Resolve band (1.8–12 keV). This Γ is consistent with the *NuSTAR* spectrum at higher energies. To model the 'soft X-ray excess', we included a warm Comptonization component (`comt`), following the approach used for NGC 3783 in Mehdipour et al. (2017). However, given that the Resolve spectrum covers only energies above 1.8 keV, the soft excess contribution is minimal (2% of the flux in the Resolve band). Nonetheless, we included the `comt` component with its parameters fixed to those of the 2001 unobscured model (Mehdipour et al. 2017).

We account for the presence of emission lines in our modeling of the Resolve spectrum. A detailed study of the Fe emission in the Resolve spectrum is presented in an upcoming paper from our campaign by Li et al. (2025b). As this paper focuses on the study of absorption by outflows, we adopt a relatively simple model for the emission lines, ensuring a well-fitted representation of both the continuum and emission features to accurately constrain the absorption lines. Our model includes the following emission features in the Resolve spectrum: Fe Kα, Fe Kβ, Ni Kα, Fe XXVI Lyα and Lyβ, Fe XXV, and S XVI Lyα. Each emission line is modeled using a delta function (`delt` in `SPEX`) convolved with a Gaussian profile (`vgau`), with multiple velocity broadening components applied as needed to achieve a good fit. The centroid of each line is fixed at zero velocity shift in the AGN rest frame, and for doublets, the expected line ratio is applied. The Gaussian velocity broadening of the lines is linked in a physically consistent manner. The velocity widths (σ_v) of the Gaussian components fitted to the Fe Kα emission line range between a few hundred to a few thousand km s^{-1}. These are broadly comparable to the widths of the Fe Kα components observed in the Resolve spectrum of NGC 4151 (XRISM Collaboration et al. 2024). The Resolve spectrum of NGC 3783 also shows the presence of a broad Fe Kα component, likely to be relativistic emission from the accretion disk (see Li et al. 2025b). For consistency, we have incorporated the relativistic emission component obtained by Li et al. (2025b), alongside our modeling of the other components using Gaussians. Our tests show that whether the broad Fe Kα emission and its associated Fe Kβ component are modeled with a relativistic or non-relativistic profile, the absorption modeling results (specifically the number of required components and their parameters) remain essentially unchanged.

3.2. Photoionized absorption modeling

Photoionization calculations were performed using the `pion` model (Mehdipour et al. 2016; Miller et al. 2015) in `SPEX`. For this, we adopted the 2001 unobscured spectral energy distribution (SED) of NGC 3783 from Mehdipour et al. (2017), which is consistent with the intrinsic UV and X-ray continuum of our observation. Using the `xabsinput` program in `SPEX`, which runs the `pion` model, we generated tables of ionic concentrations as a function of ionization parameter (ξ). These were then used by the `xabs` model (Steenbrugge et al. 2003) in `SPEX` to compute the model spectrum. To accurately reproduce all absorption features in the Resolve spectrum (Fig. 1), six `xabs` components were required. We name these components with a letter in ascending order of outflow velocity v_out, and those with comparable v_out are further sub-labeled by a number in descending order of ionization parameter ξ as shown in Table 1. The ionization parameter (ξ), column density (N_H), outflow velocity (v_out), and turbulent velocity (σ_v) of the `xabs` components were fitted. We have assumed full covering fractions for all `xabs` components, as this already provides a good fit to all lines in the Resolve spectrum.

In our model setup, all `xabs` components are illuminated by the same ionizing SED and are therefore not treated as sequential layers that shield one another. Since NGC 3783 is unobscured during our observation, there is no strong absorption of the ionizing continuum (in contrast to the obscured 2016 epoch; Mehdipour et al. 2017) that would otherwise shield components located farther out. In a layered configuration, the higher-ionization `xabs` components would be located closer to

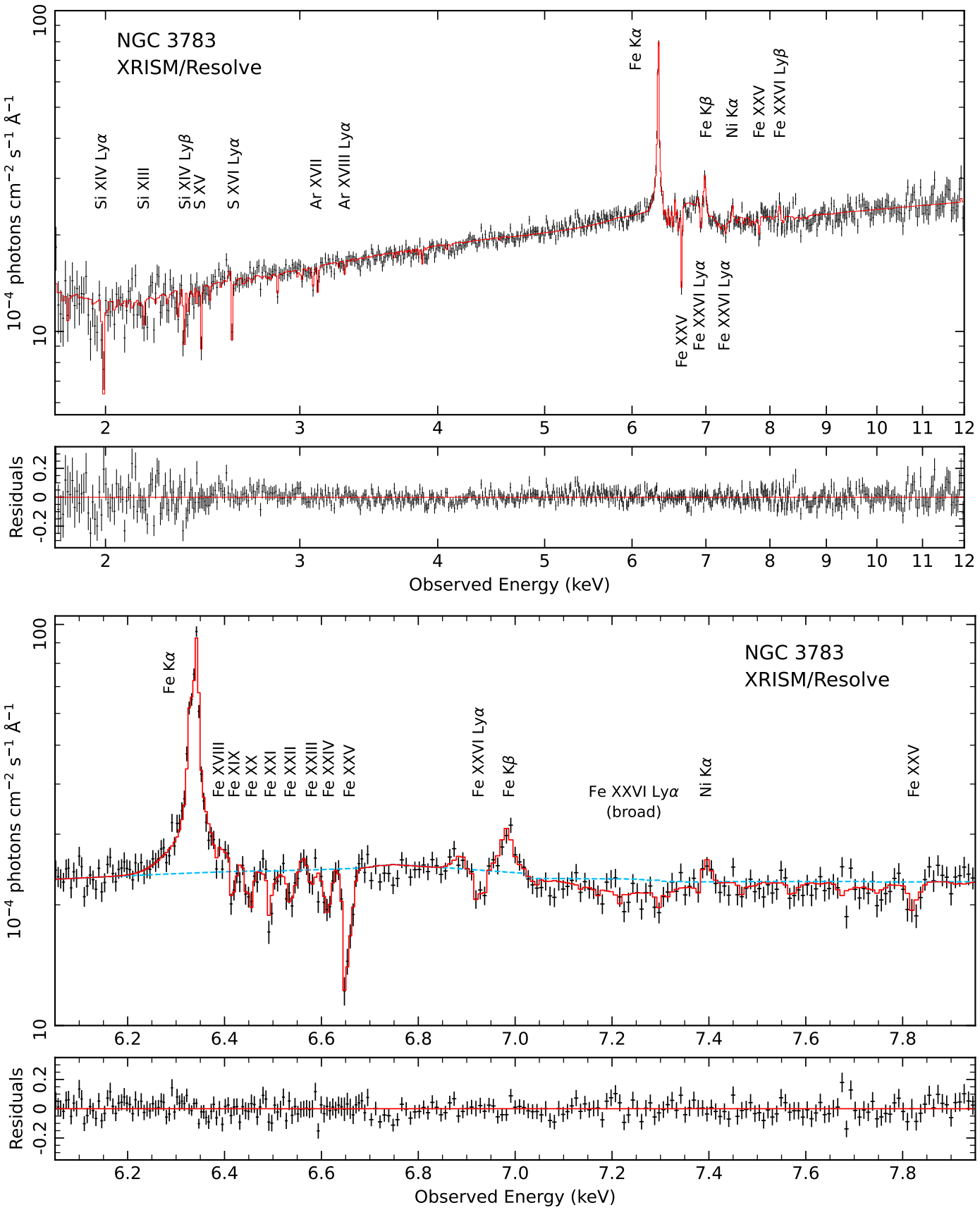

Fig. 1. XRISM/Resolve spectrum of NGC 3783 with our best-fit model. The top two panels show the full spectrum and the corresponding fit residuals. The bottom two panels provide a close-up view of the Fe K band and its fit residuals. For clarity of display the spectrum in this figure is additionally binned up. The strongest emission and absorption features are labeled. Our best-fit model (Table 1) is shown in red. The fit residuals are defined as (data − model) / model. For comparison, the blue dashed line in the third panel represents the continuum plus the broad Fe K emission, excluding any absorption lines.

the source. However, since these components have relatively low column densities and high ionization parameters, they do not significantly absorb the continuum. As a result, any shielding effect on the ionization state of the outer components would be minimal. Furthermore, as we discuss later in this paper, the outflows in NGC 3783 are found to be clumpy and structurally complex, and thus are unlikely to be arranged in simple sequential layers. Interestingly, study of obscuration in NGC 5548 (Mehdipour et al. 2024) has shown that, contrary to the shielding scenario suggested by the appearance of the UV lines, the X-ray absorption lines are unaffected by the obscuration. This indicates that the components do not cover each other in an orderly fashion.

3.3. Examination of the broad absorption component

The Resolve spectrum of NGC 3783 also shows the presence of a relatively broad dip ($\sigma_v \approx 3500$ km s^{-1}) between 7.1 and 7.4 keV (Fig. 1). The equivalent width (EW) of this feature is 17 ± 3 eV, corresponding to S/N of approximately $6\,\sigma$. We find that, regardless of how the Fe K emission is modeled (relativistic or non-relativistic), this broad residual persists below the power-law continuum, which is accurately determined by fitting the full Resolve band (1.8–12 keV) and is consistent with the *NuSTAR* spectrum at higher energies. The shape of the residual is consistent with an absorption line rather than an absorption edge. Also, at lower energies, there is no evidence for intrinsic neutral absorption in either the XRISM data or other X-ray observations from our campaign with *XMM-Newton* and *Swift*. Furthermore, no evidence for a neutral Fe K edge was previously found in the 900 ks *Chandra*/HETGS spectrum of NGC 3783 (Kaspi et al. 2002). Even during previous epochs when NGC 3783 became obscured (Mehdipour et al. 2017), the obscuring gas was significantly ionized ($\log \xi \sim 1.84$), with no neutral absorber present. We find that the strength and energy of the residual are inconsistent with either a neutral or ionized absorption edge.

We have investigated whether the broad absorption feature could instead arise from a reflection edge, but find this scenario unfeasible. Fits to the Fe Kα line using reflection models, such as the `refl` model (Magdziarz & Zdziarski 1995; Zycki et al. 1999) in `SPEX` and the `MyTorus` table model (Murphy & Yaqoob 2009), show that the associated reflected component is too weak to account for the observed trough. Our tests demonstrate that reflected/scattered emission cannot reproduce the strength or shape of the observed feature. Moreover, our modeling shows that a simple power-law fits the continuum well across the 1.8–12 keV bandpass of Resolve, with no indication of excess emission at higher energies in the spectrum. In our follow-up paper, which presents a detailed analysis of the Fe K emission in the Resolve spectrum (Li et al. 2025b), we find that the broad absorption feature persists regardless of the emission model adopted. We therefore conclude that the broad absorption trough is not the result of a reflection edge.

Adding an additional `xabs` component (named Comp. X) enables us to model the residual well as Fe XXVI Lyα, blueshifted with an outflow velocity of 14,300 km s^{-1}. Since this component is associated with a single highly ionized absorption line, its ionization parameter cannot be tightly constrained through spectral fitting. We therefore fix its ionization parameter to $\log \xi = 4.0$ based on our photoionization calculations, so that it produces only Fe XXVI. Including this component reduces the C-statistic by $\Delta C = 30$, further improving the fit. Moreover, we have compared this model from Resolve to the Xtend spectrum and find it to be fully consistent. This is demonstrated in Fig. 2, where the presence of Comp. X is evident in the Xtend spectrum. Therefore, in our spectral modeling the broad feature is consistent with Fe XXVI absorption with a sub-relativistic outflow velocity of 0.05 c.

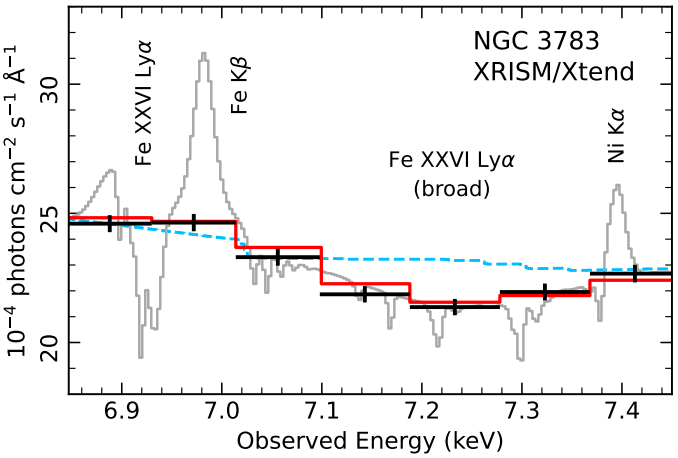

Fig. 2. XRISM/Xtend spectrum of NGC 3783 in the region of the broad Fe XXVI absorption feature of Comp. X. The Xtend data points are shown in black. Our best-fit model to the Resolve spectrum (Fig. 1 and Table 1) is shown in gray. The same model, convolved with the Xtend instrumental response, is overlaid in red. There is close agreement between this convolved model and the Xtend data, demonstrating that our Comp. X from Resolve is consistent with the Xtend data. The blue dashed line represents the continuum plus the broad Fe K emission (Sect. 3.1), under which the broad Fe XXVI absorption is evident in the Xtend spectrum, likewise seen in the Resolve spectrum (Fig. 1).

Our best-fit model and residuals are shown in Fig. 1, with the corresponding best-fit parameters listed in Table 1. The reduced C-statistic of our best fit is 1.0. The reported statistical uncertainties on the parameters correspond to the 1σ confidence level. Figure 3 illustrates the individual contribution of each `xabs` component to the overall absorption. The highest ionization components (Comps. A1, C, and X) are needed to model Fe XXVI absorption at different velocities, while most of Fe XXV absorption is produced by Comps. A1 and B. Furthermore, Comp. B is also responsible for absorption by Fe XVIII to Fe XXIV. Components A2 and A3 reproduce the lower ionization lines from Si, S, and Ar in the 1.8–3.3 keV band. The C-statistic improvement ΔC in fitting the absorption lines by each component is: 41 for Comp. A1, 129 for Comp. A2, 52 for Comp. A3, 168 for Comp. B, 31 for Comp. C, and 30 for Comp. X.

A close-up view of the absorption profile of the Fe XXV resonance line ($1s$–$2p$ transition), along with the corresponding best-fit model, is presented in Fig. 4. For comparison, the absorption profiles of the Lyα and C IV lines from the 2024 HST/COS spectrum are shown in the bottom panel of Fig. 4. Furthermore, in Fig. 5, we examine the relationships between the parameters of the six outflow components. The absorption measure distribution (AMD, Holczer et al. 2007), defined as $|\mathrm{d}N_\mathrm{H}/\mathrm{d}(\log \xi)|$, is also shown in the top panel of Fig. 5. These results are discussed in detail in the following section.

In our `SPEX` modeling, the line energies for the highly ionized Fe XXV and Fe XXVI transitions are taken from the NIST Atomic Spectra Database (Kramida et al. 2024), while those for the lower ionization species are obtained from the Flexible Atomic Code (FAC, Gu 2008). This implies uncertainties of $\sim$1 eV or better in the line energies, which do not affect the conclusions drawn from the velocities reported in Table 1.

Table 1. Best-fit parameters of the outflow components that we have determined from the XRISM Resolve spectrum of NGC 3783.

Comp.	$v_{\rm out}$ (km s^{-1})	$\log \xi$ (erg cm s^{-1})	$N_{\rm H}$ (10^{21} cm^{-2})	σ_v (km s^{-1})
A1	590 ± 30	3.19 ± 0.07	3.6 ± 0.8	40 ± 20
A2	560 ± 20	2.52 ± 0.03	11 ± 1	60 ± 20
A3	600 ± 40	1.65 ± 0.10	23 ± 2	< 10
B	700 ± 40	2.96 ± 0.07	15 ± 1	420 ± 40
C	1170 ± 100	3.56 ± 0.10	9 ± 3	250 ± 60
X	14,300 ± 1100	4.00 (f)	107 ± 14	3500 ± 1000
C-stat / expected C-stat = 3435 / 3437 ≈ 1.0				
C-stat / degrees of freedom = 3435 / 3428 ≈ 1.0				

Notes. Components are labeled with a letter in ascending order of outflow velocity $v_{\rm out}$, and those with consistent $v_{\rm out}$ are further sub-labeled by a number in descending order of ionization parameter ξ. The best-fit parameters of the power-law component (`pow`) are $\Gamma = 1.79 \pm 0.01$ with normalization of $4.16 \pm 0.06 \times 10^{51}$ photons s^{-1} keV^{-1} at 1 keV.

4. Discussion

4.1. Physical structure of the highly ionized outflows

The XRISM/Resolve spectrum of NGC 3783 has unveiled a rich array of well-resolved absorption lines, providing a detailed probe of the complex structure of the ionized outflows in this AGN. The high spectral resolution of Resolve allows the disentangling of ionization and velocity components in highly ionized outflows, a task previously unattainable. Our spectroscopic and photoionization modeling has identified six distinct absorption components, spanning a wide range of ionization states ($\log \xi$ = 1.65 to 4.0) and outflow velocities (560 to 14,300 km s^{-1}). For the first time, the high-resolution Resolve spectrum allows direct measurements of the turbulent velocity σ_v for individual absorption components. The associated photoionized emission lines appear faint in the Resolve spectrum due to both the dominance of numerous absorption lines and the likely small covering factor of the emission region.

The XRISM/Resolve studies of outflows in the quasar PDS 456 (XRISM Collaboration et al. 2025), the Seyfert-1 galaxies NGC 4151 (XRISM Collaboration et al. 2024), and NGC 3783 (this work) are commonly finding signatures of outflows in the Fe K band with similar charge states. Interestingly, these results suggest that both the UFOs and the slower highly ionized outflows in AGN are complex structures consisting of multiple ionization and velocity components. Five of the absorption components in NGC 3783 (Comps. A1 to C) are consistent with ionized outflows (the so-called warm absorbers; Yamada et al. 2024) that are typically associated with the torus and the NLR, while the broader absorption of Comp. X suggests an association with the BLR. Interestingly, the trend shown in Fig. 5 (middle panel) indicates that σ_v increases with ξ, suggesting that regions of higher ionization are associated with more dynamic and energetic gas movements. This may be because gas closer to the black hole is more highly ionized and turbulent, influenced by faster Keplerian motion in the stronger gravitational potential. Additionally, in magnetohydrodynamic (MHD) models of AGN outflows (see e.g. Fukumura et al. 2015, 2022), such relations between σ_v and ξ can be produced by magnetically driven winds.

Previously, target-of-opportunity (ToO) observations of NGC 3783 with *XMM-Newton* and HST/COS revealed that during an obscuration event in 2016, a new broad absorption feature

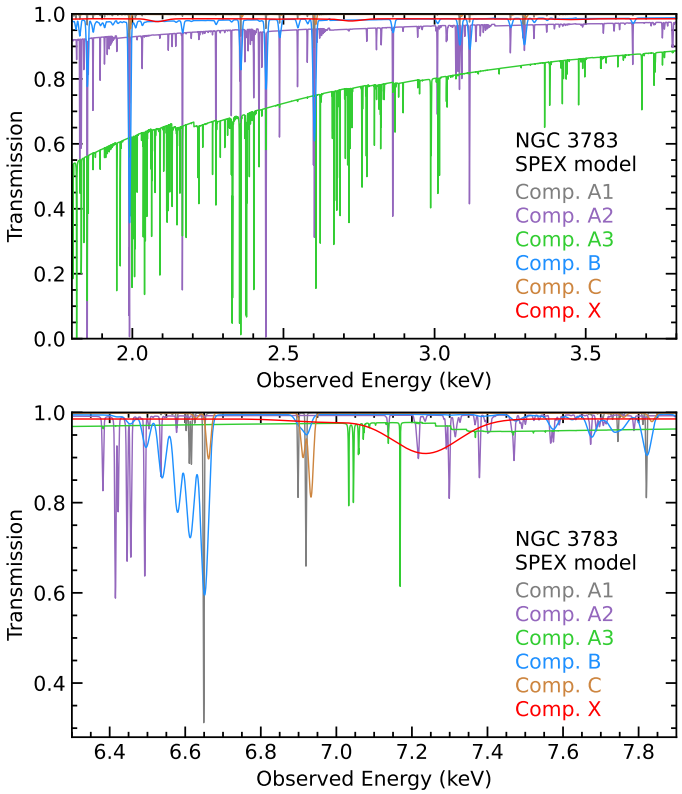

Fig. 3. Transmission model of the six outflow components. The spectra correspond to the best-fit model parameters of Table 1. Components are labeled with a letter in increasing order of outflow velocity $v_{\rm out}$, and those with similar $v_{\rm out}$ are further sub-labeled by a number in decreasing order of ionization parameter ξ.

emerged in the Fe K band (Mehdipour et al. 2017). This component exhibited an outflow velocity of 2300 km s^{-1}, similar to the broad UV absorption lines (e.g. C IV) associated with the obscurer, suggesting that the obscuring gas spans a wide range of ionization states. However, the broad absorption component detected in the 2024 Resolve spectrum is unrelated to the obscurer, as it exhibits significantly higher outflow velocities. Additionally, our 2024 X-ray observation does not show signs of obscuration. The newly identified Comp. X, which would have been challenging to detect with *XMM-Newton*, likely originates closer to the black hole than the obscurer.

The comparison of absorption line profiles for Fe XXV, C IV, and Lyα in Fig. 4 provides valuable insights and offers a model-independent way to examine their shapes. While these lines show both similarities and differences, they all exhibit absorption across a range of velocities, indicating that the outflowing gas consists of multiple velocity components. The Fe XXV profile appears asymmetric, with absorption extending to higher velocities. We note that the broadening of the Fe XXV absorption in Fig. 4 is almost entirely due to the resonance line in each of the three `xabs` components, with the contribution from the intercombination line being minimal. Nonetheless, the spectral fitting accounts for all transitions, allowing us to reliably determine the broadening of each component.

The broad and asymmetric absorption profiles observed in Fe XXVI (Figs. 1 and 2) and Fe XXV (Fig. 4) resemble the MHD wind absorption profiles predicted by the simulations of Fukumura et al. (2022), which exhibit comparable absorption troughs. Interestingly, there is also a striking resemblance between the Fe XXV and UV lines (Fig. 4), as all three exhibit their

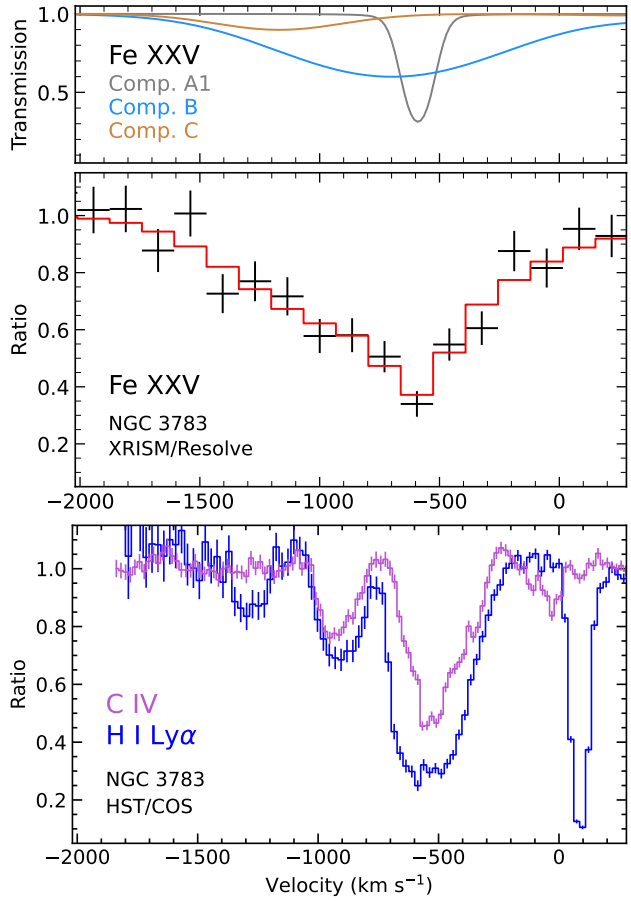

Fig. 4. Absorption profile of the Fe xxv resonance line in the XRISM Resolve spectrum compared to those of Lyα and C IV in the 2024 HST COS spectrum. The data are normalized to the continuum, showing the flux ratio on the y-axis. The red model in the middle panel corresponds to the best-fit model that is shown in Fig. 1 with its parameters given in Table 1. The top panel illustrates how the individual components of the model contribute to the Fe xxv absorption. In this figure negative velocity corresponds to an outflow, while positive corresponds to an inflow.

deepest absorption trough at the same velocity (~ -600 km s^{-1}). There is an interplay between ionization and velocity in shaping the observed absorption features. Figure 4 (top panel) shows that the highly ionized Comps. B and C of the outflows are intrinsically broader (due to higher turbulence) than their UV counterparts. This intrinsic line broadening results in blending of the spectral components. We note that while we attribute the intrinsic line broadening of each component to a single turbulence parameter, in reality, each component may have an even more complex velocity structure, resulting in 'velocity shear.' However, in practice it is challenging to constrain such details from spectral fitting alone. Nonetheless, by modeling the full XRISM/Resolve spectrum, the individual outflow components can be disentangled and parameterized, as shown in Fig. 3, the top panel of Fig. 4, and Table 1.

The bottom panel of Fig. 4 shows that Lyα traces the greatest number of absorption components. Notably, the highest velocity component at approximately –1300 km s^{-1} and the lowest at +100 km s^{-1} are observed in Lyα. The +100 km s^{-1} Lyα component likely originates from distant neutral or weakly ionized gas in the AGN's host galaxy, slowly inflowing toward the nucleus. Such a neutral or low-ionization gas would not be expected to have a corresponding high-ionization counterpart, explaining the absence of absorption in the Fe xxv profile at this velocity (Fig. 4, middle panel). Interestingly, the –1300 km s^{-1} Lyα component appears to correspond to Comp. C in X-rays, whose Fe xxv absorption model is shown in the top panel of Fig. 4. Neutral hydrogen can persist even in highly ionized gas due to its high abundance and the inhomogeneous nature of the medium. For example, Lyα counterparts of X-ray UFOs have been identified in other AGN (Kriss et al. 2018a; Mehdipour et al. 2022b). As shown in the bottom panel of Fig. 4, the Lyα outflow components are generally broader than those of C IV, suggesting that Lyα traces gas that is more turbulent and closer to the black hole. Additionally, both Fe xxv and Lyα profiles extend to higher velocities than C IV, indicating that more highly ionized gas is associated with faster outflows.

In NGC 3783, we find gas spanning a wide range of ionization states, with similar outflow velocities detected in both X-ray and UV spectra (Fig. 4). This indicates a clumpy outflow structure, in which denser (cooler) clouds are embedded within a more diffuse (hotter) medium. Such clumpy outflows are commonly seen in joint X-ray and UV spectroscopic studies of AGN (e.g. Mehdipour et al. 2022a; Zaidouni et al. 2024). Various thermal and hydrodynamic instabilities have been proposed to explain the formation of clumpy outflows in AGN (e.g. Takeuchi et al. 2013; Dannen et al. 2020; Waters et al. 2022). Alternatively, disk wind models (e.g. Fukumura et al. 2017, 2024) have been shown to reproduce the spectral characteristics of a wide range of AGN outflows, from UFOs to broad absorption (obscurers) and narrow absorption (warm absorber) outflows.

4.2. Energetics and origin of the highly ionized outflows

We derive estimates for the kinetic luminosity of the outflows, $L_{\rm kin} = 1/2\,\dot{M}_{\rm out}\,v_{\rm out}^2 = 1/2\,\mu\,m_{\rm p}\,N_{\rm H}\,R\,\Omega\,C_{\rm V}\,v_{\rm out}^3$, where $\dot{M}_{\rm out}$ is the mass outflow rate, μ the mean atomic weight per proton (≈ 1.43, from SPEX), $m_{\rm p}$ the proton mass, Ω the solid angle, $C_{\rm V}$ the volume filling factor, and R the radial distance from the source. For R, we assume minimum and maximum constraints following Blustin et al. (2005). The minimum is set by the escape velocity condition: $R \geq 2\,G\,M_{\rm BH}/v_{\rm out}^2$, where the black hole mass $M_{\rm BH} = 2.82 \times 10^7\ M_\odot$ (Bentz et al. 2021). The maximum is based on a thin-shell scenario: $R \leq L_{\rm ion}\,C_{\rm V}/(\xi\,N_{\rm H})$, where the 1–1000 Ryd ionizing luminosity $L_{\rm ion} = 6.4 \times 10^{43}$ erg s^{-1} (Mehdipour et al. 2017) is from the SED described in Sect. 3.2. We adopt a time-averaged bolometric luminosity of $L_{\rm bol} = 2.1 \times 10^{44}$ erg s^{-1} from the broadband continuum modeling of Mehdipour et al. (2017). This corresponds to an Eddington luminosity ratio of $L_{\rm bol}/L_{\rm Edd} = 0.06$. Using a fiducial value of $\Omega \sim 2\pi$ (Crenshaw & Kraemer 2012), and a volume filling factor $C_{\rm V} \sim 0.2$ (XRISM Collaboration et al. 2025) from similarly clumpy, highly ionized outflows in PDS 456, we find that for Comp. X, $L_{\rm kin}/L_{\rm bol}$ ranges from 0.008 to 0.03. This suggests that Comp. X can contribute significantly to AGN feedback, which requires $L_{\rm kin}/L_{\rm bol} \gtrsim 0.005$ (Hopkins & Elvis 2010). Using the minimum and maximum values of R for Comp. X ($0.4–1.2 \times 10^{16}$ cm), its inferred density $n_{\rm H} \sim N_{\rm H}/(C_{\rm V}\,R) \sim 0.4–1.5 \times 10^8$ cm^{-3} is interestingly similar to that of the clumps in the UFOs of PDS 456 ($n_{\rm H} \sim N_{\rm H}/d_{\rm clump} \sim 0.8–6.7 \times 10^8$ cm^{-3}; XRISM Collaboration et al. 2025). For the other slower components in NGC 3783 (Comps. A to C), $L_{\rm kin}$ is much smaller, with a combined $L_{\rm kin}/L_{\rm bol}$ of 0.0002–0.0006. This means that, even assuming these slower components are escaping winds (with some

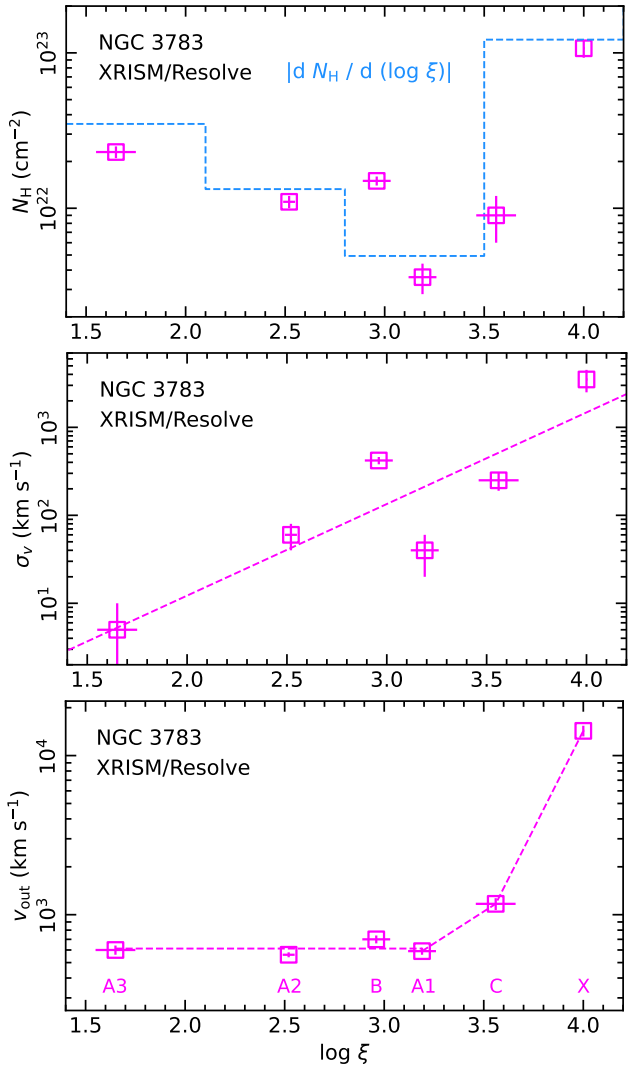

Fig. 5. Relations between the parameters of the six outflow components derived from the XRISM Resolve spectrum of NGC 3783. The top panel displays the column density N_H and the AMD as functions of the ionization parameter ($\log \xi$). The middle and bottom panels show the turbulent velocity (σ_v) and outflow velocity (v_{out}) as functions of $\log \xi$, respectively. The component label (Table 1) for each data point is shown along the lower edge of the bottom panel.

possibly being failed winds), their kinetic luminosity is nonetheless insignificant in either scenario.

The relations in Fig. 5 provide further insight into the properties of outflows observed with XRISM. The AMD is a powerful tool for probing the multi-phase nature of AGN outflows (Holczer et al. 2007; Behar 2009; Stern et al. 2014; Adhikari et al. 2019). The radial density of the outflow, as inferred from the AMD, is useful for linking observations to physical models of AGN wind launching and driving mechanisms. The AMD derived from XRISM/Resolve (Fig. 5, top panel) offers significantly greater detail, especially at higher ionization parameters, compared to those obtained with previous X-ray missions. Our results reveal that N_H and the AMD generally decline from $\log \xi = 1.65$ to 3.2, before rising at higher ionization parameters (Fig. 5, top panel). While a roughly flat AMD shape in the lower-ionization regime ($\log \xi < 3.2$) cannot be conclusively ruled out, nonetheless, our interpretation of the AMD (discussed below) remains unchanged regardless of whether the shape is declining or flat. Additionally, we emphasize that the significant increase in N_H due to Comp. X is robust, despite its ionization parameter being fixed to the minimum feasible ξ in our modeling, as a higher ξ would require an even greater N_H. Interestingly, while the faster outflow components generally exhibit higher turbulent velocities (Table 1), a significant jump in the outflow velocity is observed above $\log \xi = 3.2$ (Fig. 5, bottom panel). These AMD and velocity trends are not easily attributable to a single wind-driving mechanism, pointing instead to a more complex outflow structure in NGC 3783.

Our results point to the presence of a 'hybrid wind,' giving rise to two distinct patterns in the lower-ionization and higher-ionization regimes. The declining AMD trend at lower ionization ($\log \xi < 3.2$) is consistent with thermally driven winds, as shown by Dyda et al. (2017), while the increasing trend at higher ionization ($\log \xi > 3.2$) aligns with expectations for magnetically driven winds (e.g., Fukumura et al. 2015). Moreover, the significant increase in outflow velocity at higher ionization further supports this interpretation, in which the slower outflows are thermal winds (e.g., Mizumoto et al. 2019) and the faster outflows are magnetic winds (e.g., Fukumura et al. 2010). Thermally driven winds are inherently slow, typically outflowing at hundreds of km s^{-1} (e.g. Ganguly et al. 2021), consistent with our Comps. A1, A2, A3, and B. In contrast, magnetically driven winds can reach velocities of several thousand km s^{-1}, and in some cases, reach relativistic speeds, in line with our Comps. C and X. Therefore, our findings suggest that the absorption along our line of sight originates from two distinct regions: a highly ionized, magnetically driven disk wind, surrounded by thermally driven ionized outflows farther out. We note that radiatively driven outflows (e.g. Proga et al. 2000; Giustini & Proga 2019; Waters et al. 2021; Mizumoto et al. 2021) can also contribute significantly in the 'hybrid wind' scenario that we observe in NGC 3783. In this Paper I of our series, we have focused on the kinematic and ionization structure of the highly ionized outflows in the time-averaged XRISM/Resolve spectrum. To gain a more complete understanding, all phases of the outflows, including those in the soft X-ray (*XMM-Newton*/RGS) and UV (HST/COS), must be studied alongside the XRISM/Resolve results. In our follow-up papers, we plan to carry out such a multi-wavelength investigation.

5. Conclusions

Our XRISM/Resolve analysis of NGC 3783 reveals multi-component, highly ionized outflows in this AGN. We identify six absorption components: five with relatively narrow absorption lines and moderate outflow velocities (560–1170 km s^{-1}), and one broad absorption component outflowing at sub-relativistic speeds ($0.05\,c$). With a kinetic luminosity of 0.8–3% of the bolometric luminosity, this sub-relativistic component is likely to be energetically significant for AGN feedback. The Resolve spectrum shows that higher-ionization absorption lines (such as Fe XXVI and Fe XXV) are generally broader than those of lower-ionization species, suggesting that the gas closer to the black hole is more highly ionized and exhibits higher turbulence, likely due to increased Keplerian motion in the deeper gravitational potential. Additionally, the column density N_H generally decreases with the ionization parameter from $\log \xi = 1.65$ to 3.2, but significantly increases at higher values, hinting at a complex ionization structure along our line of sight. Comparing the kinematics of the highly ionized outflows with the UV absorption lines (Lyα and C IV) observed by HST/COS reveals that gas across a wide range of ionization states outflows at similar velocities, which is indicative of a clumpy, multi-zone outflow structure.

The trends observed by XRISM/Resolve between the parameters of the outflow components in the lower and higher ionization regimes suggest a 'hybrid wind' scenario, in which a faster, magnetically driven disk wind is surrounded by slower, thermally driven outflows extending further out. These findings demonstrate the power of high-resolution X-ray spectroscopy in the Fe K band for probing AGN winds. When combined with multiwavelength observations of the outflows, they provide crucial insights into the structure and driving mechanisms of AGN outflows.

Acknowledgements. M. Mehdipour acknowledges support from NASA XRISM Guest Scientist (XGS) grant (80NSSC23K0995). This work is also supported by NASA through a grant for HST program number 17273 from the Space Telescope Science Institute, which is operated by the Association of Universities for Research in Astronomy, Incorporated, under NASA contract NAS5-26555. Support from NASA NuSTAR grant 80NSSC25K7126 is acknowledged. SRON is supported financially by NWO, the Netherlands Organization for Scientific Research. Part of this work was performed under the auspices of the U.S. Department of Energy by Lawrence Livermore National Laboratory under Contract DE-AC52-07NA27344. K.F. acknowledges support from NASA XGS grant (80NSSC23K1021). This work was supported by JSPS KAKENHI Grant Number JP21K13958. M. Mizumoto acknowledges support from Yamada Science Foundation. We thank G. Kriss, C. Done, L. Gallo, M. Leutenegger, and R. Mushotzky for valuable discussions and helpful feedback. The anonymous referee is acknowledged for their constructive comments and suggestions, which improved the paper.

References

Adhikari, T. P., Różańska, A., Hryniewicz, K., Czerny, B., & Behar, E. 2019, ApJ, 881, 78
Behar, E. 2009, ApJ, 703, 1346
Behar, E., Rasmussen, A. P., Blustin, A. J., et al. 2003, ApJ, 598, 232
Bentz, M. C., Williams, P. R., Street, R., et al. 2021, ApJ, 920, 112
Blustin, A. J., Page, M. J., Fuerst, S. V., Branduardi-Raymont, G., & Ashton, C. E. 2005, A&A, 431, 111
Costanzo, D., Dadina, M., Vignali, C., et al. 2022, A&A, 659, A161
Crenshaw, D. M. & Kraemer, S. B. 2012, ApJ, 753, 75
Dannen, R. C., Proga, D., Waters, T., & Dyda, S. 2020, ApJ, 893, L34
de Plaa, J., Kaastra, J. S., Tamura, T., et al. 2004, A&A, 423, 49
Dyda, S., Dannen, R., Waters, T., & Proga, D. 2017, MNRAS, 467, 4161
Eckart, M. E., Brown, G. V., Chiao, M. P., et al. 2024, in Space Telescopes and Instrumentation 2024: Ultraviolet to Gamma Ray, ed. J.-W. A. den Herder, S. Nikzad, & K. Nakazawa, Vol. 13093, International Society for Optics and Photonics (SPIE), 130931P
Fox, A., James, B., Roman-Duval, J., Rafelski, M., & Sonnentrucker, P. 2018, The Spectral Resolution of the COS FUV channel at Lifetime Position 4, Instrument Science Report COS 2018-7
Fukumura, K., Dadina, M., Matzeu, G., et al. 2022, ApJ, 940, 6
Fukumura, K., Kazanas, D., Contopoulos, I., & Behar, E. 2010, ApJ, 715, 636
Fukumura, K., Kazanas, D., Shrader, C., et al. 2017, Nature Astronomy, 1, 0062
Fukumura, K., Mehdipour, M., Behar, E., et al. 2024, ApJ, 968, 70
Fukumura, K., Tombesi, F., Kazanas, D., et al. 2015, ApJ, 805, 17
Gabel, J. R., Kraemer, S. B., Crenshaw, D. M., et al. 2005, ApJ, 631, 741
Gallo, L. C., Miller, J. M., & Costantini, E. 2023, arXiv e-prints, arXiv:2302.10930
Ganguly, S., Proga, D., Waters, T., et al. 2021, ApJ, 914, 114
Gaspari, M. & Sądowski, A. 2017, ApJ, 837, 149
Giustini, M. & Proga, D. 2019, A&A, 630, A94
Gu, L., Kaastra, J., Rogantini, D., et al. 2023, A&A, 679, A43
Gu, M. F. 2008, Canadian Journal of Physics, 86, 675
Holczer, T., Behar, E., & Kaspi, S. 2007, ApJ, 663, 799
Hopkins, P. F. & Elvis, M. 2010, MNRAS, 401, 7
Ishisaki, Y., Yamada, S., Seta, H., et al. 2018, Journal of Astronomical Telescopes, Instruments, and Systems, 4, 011217
Kaastra, J. S. & Bleeker, J. A. M. 2016, A&A, 587, A151
Kaastra, J. S., Mewe, R., & Nieuwenhuijzen, H. 1996, in UV and X-ray Spectroscopy of Astrophysical and Laboratory Plasmas, ed. K. Yamashita & T. Watanabe (Tokyo: Univ. Academy Press), 411–414
Kaastra, J. S., Raassen, A. J. J., de Plaa, J., & Gu, L. 2024, SPEX X-ray spectral fitting package v3.08.01, Zenodo, https://doi.org/10.5281/zenodo.12771915
Kaspi, S., Brandt, W. N., George, I. M., et al. 2002, ApJ, 574, 643
King, A. & Pounds, K. 2015, ARA&A, 53, 115
Kramida, A., Yu. Ralchenko, Reader, J., & and NIST ASD Team. 2024, NIST Atomic Spectra Database (version 5.12), [Online]. Available: https://physics.nist.gov/asd . National Institute of Standards and Technology, Gaithersburg, MD. DOI: https://doi.org/10.18434/T4W30F
Kriss, G. A., Lee, J. C., Danehkar, A., et al. 2018a, ApJ, 853, 166
Kriss, G. A., Mehdipour, M., Kaastra, J. S., et al. 2019, A&A, 621, A12
Laha, S., Guainazzi, M., Dewangan, G. C., Chakravorty, S., & Kembhavi, A. K. 2014, MNRAS, 441, 2613
Laha, S., Reynolds, C. S., Reeves, J., et al. 2021, Nature Astronomy, 5, 13
Li, C., Kaastra, J. S., Gu, L., et al. 2025, A&A, 694, A302
Li et al. 2025b, A&A
Lodders, K., Palme, H., & Gail, H. P. 2009, Landolt Börnstein, 4B, 712
Magdziarz, P. & Zdziarski, A. A. 1995, MNRAS, 273, 837
Mao, J., Mehdipour, M., Kaastra, J. S., et al. 2019, A&A, 621, A99
Mehdipour, M., Kaastra, J. S., & Kallman, T. 2016, A&A, 596, A65
Mehdipour, M., Kaastra, J. S., Kriss, G. A., et al. 2017, A&A, 607, A28
Mehdipour, M., Kriss, G. A., Costantini, E., et al. 2022a, ApJ, 934, L24
Mehdipour, M., Kriss, G. A., Kaastra, J. S., et al. 2024, ApJ, 962, 155
Mehdipour, M., Kriss, G. A., Krongold, Y., et al. 2022b, ApJ, 930, 166
Miller, J. M., Kaastra, J. S., Miller, M. C., et al. 2015, Nature, 526, 542
Mizumoto, M., Done, C., Tomaru, R., & Edwards, I. 2019, MNRAS, 489, 1152
Mizumoto, M., Nomura, M., Done, C., Ohsuga, K., & Odaka, H. 2021, MNRAS, 503, 1442
Mochizuki, Y., Tsujimoto, M., Kilbourne, C. A., et al. 2025, Journal of Astronomical Telescopes, Instruments, and Systems, 11, 042002
Murphy, E. M., Lockman, F. J., Laor, A., & Elvis, M. 1996, ApJS, 105, 369
Murphy, K. D. & Yaqoob, T. 2009, MNRAS, 397, 1549
Noda, H., Mori, K., Tomida, H., et al. 2025, PASJ[arXiv:2502.08030]
Porter, F. S., Kilbourne, C. A., Chiao, M., et al. 2024, in Space Telescopes and Instrumentation 2024: Ultraviolet to Gamma Ray, ed. J.-W. A. den Herder, S. Nikzad, & K. Nakazawa, Vol. 13093, International Society for Optics and Photonics (SPIE), 130931K
Proga, D., Stone, J. M., & Kallman, T. R. 2000, ApJ, 543, 686
Reeves, J. N., Nandra, K., George, I. M., et al. 2004, ApJ, 602, 648
Scott, A. E., Brandt, W. N., Behar, E., et al. 2014, ApJ, 797, 105
Steenbrugge, K. C., Kaastra, J. S., Crenshaw, D. M., et al. 2005, A&A, 434, 569
Steenbrugge, K. C., Kaastra, J. S., de Vries, C. P., & Edelson, R. 2003, A&A, 402, 477
Stern, J., Behar, E., Laor, A., Baskin, A., & Holczer, T. 2014, MNRAS, 445, 3011
Takeuchi, S., Ohsuga, K., & Mineshige, S. 2013, PASJ, 65, 88
Tashiro, M., Kelley, R., Watanabe, S., et al. 2025, PASJ
Tashiro, M., Maejima, H., Toda, K., et al. 2020, in Society of Photo-Optical Instrumentation Engineers (SPIE) Conference Series, Vol. 11444, Space Telescopes and Instrumentation 2020: Ultraviolet to Gamma Ray, ed. J.-W. A. den Herder, S. Nikzad, & K. Nakazawa, 1144422
Theureau, G., Bottinelli, L., Coudreau-Durand, N., et al. 1998, A&AS, 130, 333
Tombesi, F., Cappi, M., Reeves, J. N., et al. 2010, A&A, 521, A57
Waters, T., Proga, D., & Dannen, R. 2021, ApJ, 914, 62
Waters, T., Proga, D., Dannen, R., & Dyda, S. 2022, ApJ, 931, 134
XRISM Collaboration. 2025c, Paper II, A&A
XRISM Collaboration, Audard, M., Awaki, H., et al. 2024, ApJ, 973, L25
XRISM Collaboration, Audard, M., Awaki, H., et al. 2025, Nature, 641, 1132
XRISM TTWOF. 2025, Things to watch out for with XRISM data processing and analysis, https://heasarc.gsfc.nasa.gov/docs/xrism/analysis/ttwof/index.html
Yamada, S., Kawamuro, T., Mizumoto, M., et al. 2024, ApJS, 274, 8
Yaqoob, T., Reeves, J. N., Markowitz, A., Serlemitsos, P. J., & Padmanabhan, U. 2005, ApJ, 627, 156
Zaidouni, F., Kara, E., Kosec, P., et al. 2024, ApJ, 974, 91
Zycki, P. T., Done, C., & Smith, D. A. 1999, MNRAS, 305, 231

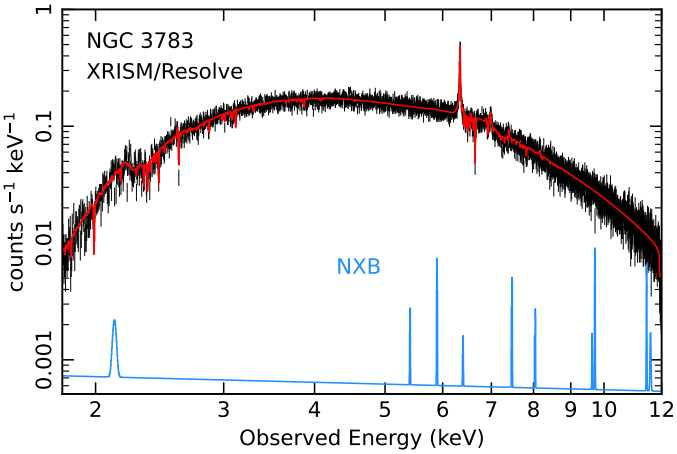

Fig. A.1. Comparison of the count rate spectra of the source (black) and the NXB (blue) in the XRISM/Resolve observation of NGC 3783. The best-fit model, described in Sect. 3, is shown in red. The NXB contribution across the bandpass is mostly minimal.

Appendix A: Non-X-ray Background in the Resolve Spectrum of NGC 3783

We show in Fig. A.1 the XRISM/Resolve count rate spectrum of NGC 3783, together with the corresponding Non-X-ray Background (NXB) model. The NXB contribution is mostly minimal, becoming marginally relevant toward the ends of the bandpass. Additional details on the Resolve data reduction and NXB modeling are provided in Sect. 2.1 and XRISM Collaboration (2025c, Paper II).